Title

Proteome-Wide Characterizations of N 6-Methyl-Adenosine Triphosphate- and N 6-Furfuryl-Adenosine Triphosphate-Binding Capabilities of Kinases

Journal

Analytical Chemistry, 93(39)

ISSN

0003-2700

Authors

Dong, Xuejiao
Sun, Jianan
Miao, Weili
et al.

Publication Date

2021-10-05

DOI

10.1021/acs.analchem.1c02565

Peer reviewed

HHS Public Access

Author manuscript

Anal Chem. Author manuscript; available in PMC 2022 October 05.

Published in final edited form as:

Anal Chem. 2021 October 05; 93(39): 13251–13259. doi:10.1021/acs.analchem.1c02565.

Proteome-Wide Characterizations of N^6-Methyl-Adenosine Triphosphate- and N^6-Furfuryl-Adenosine Triphosphate-Binding Capabilities of Kinases

Xuejiao Dong,
Department of Chemistry, University of California, Riverside, California 92521, United States

Jianan Sun,
Environmental Toxicology Graduate Program, University of California, Riverside, California 92521, United States

Weili Miao,
Department of Chemistry, University of California, Riverside, California 92521, United States

Chia-en A. Chang,
Department of Chemistry, University of California, Riverside, California 92521, United States

Yinsheng Wang
Department of Chemistry and Environmental Toxicology Graduate Program, University of California, Riverside, California 92521, United States

Abstract

Kinases catalyze the transfer of the γ-phosphate group from adenosine triphosphate (ATP) to their protein and small-molecule substrates, and this phosphorylation is a crucial element of multiple cell signaling pathways. Herein, we employed isotope-coded ATP acyl-phosphate probes, in conjunction with a multiple-reaction monitoring (MRM)-based targeted proteomic method for proteome-wide identifications of endogenous kinases that can bind to two N^6-modified ATP derivatives, N^6-methyl-ATP (N^6-Me-ATP), and N^6-furfuryl-ATP (a.k.a. kinetin triphosphate, KTP). We found that, among the ~300 quantified kinases, 27 and 18 are candidate kinases that can bind to KTP and N^6-Me-ATP, respectively. Additionally, GSK3α and GSK3β are among the kinases that can bind to both ATP analogues. Moreover, the *in vitro* biochemical assay showed that GSK3β could employ N^6-Me-ATP but not KTP as the phosphate group donor

Corresponding Author: Phone: (951)827-2700; yinsheng.wang@ucr.edu.

ASSOCIATED CONTENT

Supporting Information

The proteomic data were deposited into PeptideAtlas with the identifier number of PASS01695 (http://www.peptideatlas.org/PASS/PASS01695) The Supporting Information available free of charge at https://pubs.acs.org/doi/10.1021/acs.analchem.1c02565.

Experimental procedures for recombinant protein generation, *in vitro* kinase assay and molecular docking; MS data for *in vitro* kinase reaction; image and FPLC trace for monitoring protein purification; and MD simulation results (PDF)

Identification data for all peptides and proteins in the kinase MRM library with capabilities in binding toward N^6-Me-ATP based on the desthiobiotin-C3-ATP probes vs N^6-Me-ATP competition experiment (XLSX)

Identification data for all peptides and proteins in the kinase MRM library with capabilities in binding toward KTP based on the desthiobiotin-C3-ATP probes vs KTP competition experiment (XLSX)

The authors declare no competing financial interest.

Complete contact information is available at: https://pubs.acs.org/10.1021/acs.analchem.1c02565

to phosphorylate its substrate peptide. Molecular modeling studies provided insights into the differences between N^6-Me-ATP and KTP in enabling the GSK3β-mediated phosphorylation. Together, our chemoproteomic approach led to the identification of endogenous kinases that can potentially be targeted by the two ATP analogues. The approach should be generally applicable for assessing endogenous kinases targeted by other ATP and purine analogues.

Graphical Abstract

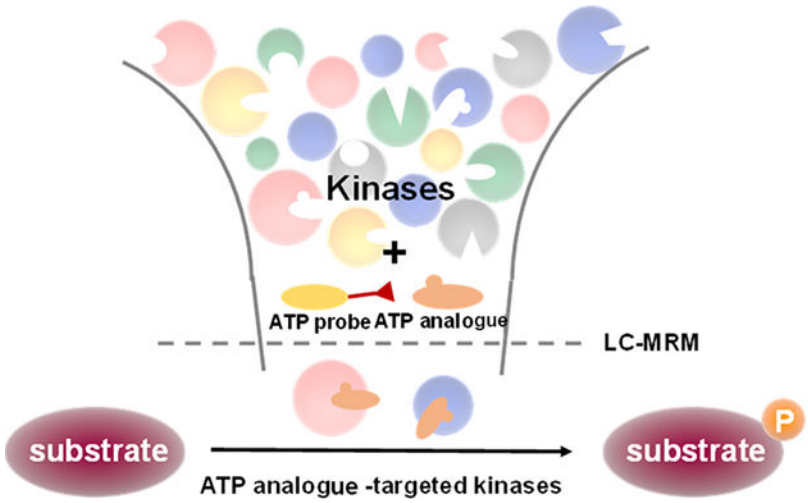

INTRODUCTION

Protein kinases are encoded by more than 500 distinct genes, which constitute approximately 2% of all protein-coding human genes.[1–3] Studies in the last several decades established central roles of protein kinases in the regulation of crucial biological processes, including cell signaling, proliferation, and metabolism.[4,5] Amplifications, mutations, and abnormal expression/activation of kinase genes are associated with and contribute to human diseases.[1,4] Therefore, kinase inhibitors and kinase-substrate interactions have been intensively investigated and exploited for the therapeutic interventions of various human diseases.[6]

Multiple kinases in different cell signaling pathways may converge on common phosphorylation sites in a substrate protein, and sequential phosphorylations may occur in kinase-mediated signaling cascades, which render it very challenging to identify direct substrates for specific kinases.[7–9] To address this challenge, Shokat *et al.*[10,11] introduced a creative approach, termed analogue-specific kinases, to define kinase-substrate relationships. This approach harnesses the power of chemical syntheses of N^6-modified adenosine triphosphate (ATP) analogues or purine analogues and genetic engineering of the kinase of interest to accommodate these analogues for substrate phosphorylation. We reason that it is important to assess, at the proteome-wide scale, whether these analogue substrates can also be recognized by endogenous kinases. Such characterizations of endogenous kinases that can recognize the ATP/purine analogues are important for rigorous interpretation of data obtained from the analogue-specific kinases, where substrates phosphorylated by these off-

target endogenous kinases may yield false-positive results. Additionally, the results obtained from these characterizations may also provide an opportunity to discover substrates for native kinases in cells. In this vein, N^6-furfuryl-ATP (a.k.a. kinetin triphosphate, KTP) was found to enhance the activity of wild-type PINK1 kinase and restore the catalytic activity of a Parkinson's disease-related mutant (*i.e.*, G309D) of PINK1 to near-wild-type levels.[11]

Targeted proteomics, relying on multiple-reaction monitoring (MRM) on a triple-quadrupole mass spectrometer or parallel-reaction monitoring (PRM) on an Orbitrap mass spectrometer, have the attributes of providing enhanced sensitivity, reproducibility, and accuracy relative to discovery proteomics.[12,13] Recently a scheduled MRM-based targeted proteomic method, along with the use of isotope-coded desthiobiotin-ATP acyl phosphate probes, was employed for proteome-wide assessment of ATP-binding capabilities of kinases. The chemoproteomic method facilitates high-throughput interrogation of approximately 300 human kinases.[14]

In this study, we applied the chemoproteomic approach to examine the relative abilities of the human kinome in binding to N^6-methyl-ATP (N^6-Me-ATP) and KTP versus native ATP (Figure 1a). We also revealed the ability of N^6-Me-ATP, but not KTP, as a phosphate group donor for GSK3β, one of the kinases that can bind to both nucleotide analogues, to phosphorylate its substrate peptide. Furthermore, we employed molecular dynamics (MD) simulations to understand the differences in interactions between GSK3β and N^6-Me ATP and KTP.

EXPERIMENTAL SECTION

Cell Culture.

HEK293T cells were cultured in Dulbecco's modified Eagle medium (DMEM, Gibco) supplemented with 10% fetal bovine serum (FBS, Corning), 100 U/mL penicillin, and 100 μg/mL streptomycin (Cytiva). The cells were maintained in a humidified atmosphere with 5% CO_2 at 37 °C, and the culture medium was changed in every 2–3 days as needed.

Sample Preparation and Isotope-Coded ATP Affinity Probe Labeling.

HEK293T cells were harvested at ~80% confluency and washed 3 times with cold PBS. The cells were then lysed by incubating at 0 °C for 30 min, in a buffer containing 50 mM 4-(2-hydroxyethyl)-1-piperazineethanesulfonic acid (HEPES, pH 7.4), 100 mM NaCl, 0.5 mM EDTA, 0.7% CHAPS, and a protease inhibitor cocktail (1:100, v/v). The resulting mixture was centrifuged at 16000*g* and 4 °C for 30 min. After removal of endogenous nucleotides using a NAP-10 column (Amersham Biosciences), proteins were eluted into a buffer containing 50 mM HEPES (pH 7.4), 75 mM NaCl, and 5% glycerol. Protein concentrations in the resultant lysates were subsequently quantified by the Quick Start Bradford protein assay (Bio-Rad, Hercules, CA).

The isotope-labeled desthiobiotin-C3-ATP probes were synthesized previously.[15] $MgCl_2$, $MnCl_2$, and $CaCl_2$ were added to the concentrated protein lysate immediately before the labeling reaction, and their final concentrations were 50, 5, and 5 mM, respectively. The resulting protein lysates (1.5 mg each) were incubated with or without 100 μM N^6-Me-ATP or KTP at 4 °C for 20 min. A heavy or light isotope-coded ATP affinity probe (100 μM) was

subsequently added to the reaction mixture and incubated at room temperature with gentle shaking for 2 h. The reactions were terminated by adding glycine until its final concentration was 50 mM. After incubation at room temperature for another 20 min, heavy and light ATP probe-labeled cell lysates were mixed at a 1:1 ratio (w/w).

For the concentration-dependent competition experiments, 1.5 mg of the protein lysate was preincubated separately with 10, 100, and 200 μM N^6-Me-ATP or KTP, followed by incubation with 100 μM heavy ATP affinity probe, in which the same amount of the lysate was incubated with 100 μM light ATP-affinity probe alone. The subsequent steps of sample preparation were the same as described above.

After ATP affinity probe labeling, the protein samples were subjected to filter-aided sample preparation (FASP).[16] The desthiobiotin-conjugated peptides were enriched from the ensuing tryptic digestion mixture with high-capacity streptavidin beads (Sigma-Aldrich) and desalted using C18 pipette tips (Agilent), as described elsewhere.[15]

Scheduled LC-MRM Analysis.

Scheduled LC-MRM experiments were performed on a TSQ Altis triple-quadrupole mass spectrometer (Thermo Fisher, San Jose, CA) equipped with a nanoelectrospray ionization source, which was coupled to an UltiMate 3000 UPLC RSLCnano system (Dionex, Thermo Fisher), with the detailed conditions provided in the online Supporting Information. The details about the purification of recombinant GSK3β and the *in vitro* kinase assay are also provided in Supporting Information.

MD Simulations.

The initial structure for GSK3β was downloaded from the Protein Data Bank (ID: 1PYX).[17] The initial positions of the ligands ATP, KTP, and N^6-Me-ATP in MD simulations were superimposed to those of AMP-PNP in 1PYX. The Amber18 package with GPU implementation was used for unbiased all-atom MD simulations.[18] The Amber FF99SB and Li/Merz ion parameters were employed for GSK3β and Mg^{2+} ion, respectively.[19,20] ATP force field parameters and partial charges were obtained from an existing publication using quantum mechanics at the RHF/6–31+G* level of theory.[21] Partial charges for adductions in KTP and N^6-Me-ATP were calculated using the am1-bcc method, and general AMBER force field was used for the force field parameters of adductions.[22] The force field parameters and partial charges for adenine, ribose, and triphosphate in KTP and N^6-Me-ATP were taken from the corresponding parameters of ATP. A Mg^{2+} ion was placed between a ligand and protein to maintain the positions of ATP phosphates. Minimization of hydrogen atoms, the side chains, and the entire system was executed for 500, 5000, and 3000 steps, respectively. The system was placed under the implicit Hawkins, Cramer, Truhlar pairwise generalized Born (GB) model.[23,24] The system was then slowly heated up to 50, 100, 150, 200, and 250 K for 100 ps at each temperature. A 50 ns classical MD was subsequently performed with a restrained ligand position at 298 K, which only allowed proteins to move. A Langevin thermostat was used to maintain a temperature of 298 K. Frames were saved every 10 ps with a time step of 2 fs. Finally, the SHAKE algorithm was applied to constrain the covalent bonds involving hydrogen atoms.[25]

RESULTS AND DISCUSSION

A Chemoproteomic Approach for Interrogating the N^6-Me-ATP- and KTP-Binding Capabilities of the Human Kinome.

In this study, we aim to develop a targeted proteomic strategy to evaluate, at the proteome-wide scale, the binding capabilities of kinases toward two N^6-modified ATP derivatives, that is, N^6-Me-ATP and KTP, relative to unmodified ATP. These two ATP analogues were chosen because the former represents the N^6-alkylated ATP derivative with the smallest alkyl group, and KTP was previously found to be recognized by an endogenous kinase, that is, PINK1.[11]

Our method is based on the use of the previously synthesized stable isotope-labeled desthiobiotin-ATP acyl phosphate probes (Figure 1a)[15] and a recently reported scheduled MRM method for high-throughput proteome-wide assessment of ATP-binding affinities of human kinases.[14] In particular, the kinome MRM library includes the normalized retention times (iRTs)[26] and at least three MRM transitions for each of the 818 nonredundant desthiobiotin-labeled light and heavy peptides derived from 474 kinases. The library encompasses 409 protein kinases and covers approximately 80% of the human kinome.

We first performed a competition experiment, where equal amounts of protein lysates of HEK293T cells were treated separately with 100 μM light and heavy desthiobiotin-C3-ATP probes (Figure S1) in the absence or presence of the same concentration of N^6-Me-ATP or KTP. To achieve robust quantification, we conducted both forward and reverse chemical labeling experiments, where the lysates incubated with heavy and light probes were preincubated with the ATP analogues in the forward and reverse labeling experiments, respectively (Figure 1b).

We manually checked all the quantified peptides to ensure that the signal intensity distributions of selected transitions match with those in the Skyline spectral library, with the dotp values being larger than 0.7 (Figure 2a). On the basis of full-scan MS/MS acquired from shotgun proteomic experiments, transitions for the formation of the three most abundant y-ions were selected for the scheduled MRM analysis of the corresponding light- and heavy-labeled kinase peptides (*e.g.*, the y_7, y_8, and y_9 ions in Figure 2b). The distribution patterns of the three y-ions derived from the light- and heavy-labeled peptides in both forward and reverse replicates were very similar to those in the full-scan MS/MS in the library (Figure 2c). In addition, the observed retention times and calculated iRTs for the 263 quantified desthiobiotin-conjugated peptides exhibited excellent linear correlations (Figure 2d). Moreover, the peptide intensity ratios obtained from forward and reverse labeling experiments are consistent for the quantified peptides (Figure 2e). These results together support the reliable identification and quantification of the kinase peptides.

When the ATP-binding pocket of putative ATP analogue-targeted kinases is occupied by N^6-modified ATP derivatives, it will prevent the kinase from binding with the ATP acyl phosphate probe; hence, kinases exhibiting low labeling ratios of analogue-treated/untreated samples are considered the candidate target kinases for the ATP analogues (Figure 2e). The target kinases of the tested ATP analogues are shown in the bottom quadrant of the scatter

plots displaying the logarithmic (log_2) ratios of the identified kinases in forward and reverse labeling experiments.

The LC-MRM results enabled the quantification of 300 unique peptides derived from 215 kinases from the N^6-Me-ATP competition experiments and 306 distinct peptides representing 218 kinases from the KTP competition experiments (Tables S1 and S2). As expected, most kinases exhibit labeling ratios that are close to unity, revealing their preferential binding to ATP than its N^6-modified counterparts. We attempted to include all the putative kinases that can accept the two ATP analogues; hence, we employed a lenient criterion, with the analogue-treated/untreated ratio being lower than 0.75. With this criterion, our competition experiments led to the identifications of 27 and 18 kinases with capabilities of binding toward KTP (Table 1) and N^6-Me-ATP (Table 2), respectively. Among them, nine kinases were targeted by both ATP analogues, including two isoforms of glycogen synthase kinase-3 (GSK3α and GSK3β), where in N^6-Me-ATP and KTP competition experiments, GSK3α displays ratios of ~0.55 and ~0.61, respectively, and GSK3β exhibits ratios of 0.54 and 0.72, respectively (Tables 1 and 2, Figures 3 and S4). GSK3α and GSK3β are key kinases contributing to aberrant phosphorylation in Alzheimer's disease.[27,28] In addition, these kinases can be inhibited by lithium,[29,30] and lithium is a mood stabilizer used in the treatment of bipolar disorder.[31]

Another targeted kinase, eukaryotic elongation factor 2 kinase (eEF2K), exhibits ratios of 0.60 and 0.69 in KTP and N^6-Me-ATP competition experiments, respectively (Tables S1 and S2). eEF2K is an atypical protein kinase that phosphorylates and inactivates eEF2, thereby negatively regulating translation elongation.[32] In addition, a tryptic peptide derived from CSKN2A2 (α2 subunit of casein kinase 2), that is, VLGTEELYGYLKK, exhibits a ratio of 0.70 in the KTP competition experiment (Table S2). This result is in accordance with a previous observation that KTP can support the casein kinase 2-mediated phosphorylation of the Huntingtin N17 domain.[33]

To further validate that the diminution in ATP-probe labeling efficiency is dependent on the interaction between the ATP analogues and kinase, we next asked if the labeling efficiencies for the kinases decrease with the concentrations of the ATP analogues. To this end, we preincubated the same amount of the protein lysate of HEK293T cells individually with 10, 100, or 200 μM ATP analogues and subsequently labeled the lysate with 100 μM heavy ATP acyl phosphate probe, whereas the same amount of the protein lysate without preincubation with the ATP analogue was incubated with 100 μM light ATP probe.

Our results showed that the ATP probe labeling efficiency of GSK3α gradually decreases with increasing concentrations of KTP or N^6-Me-ATP (Figure 4). For instance, the ATP probe labeling efficiencies for GSK3α decreased by 15, 44, and 64% when the lysate was preincubated with 10, 100, and 200 μM N^6-Me-ATP, respectively (Figure 4a–c). This result indicates that GSK3α exhibits similar binding affinities toward N^6-Me-ATP and ATP. The corresponding experiments with KTP revealed drops in labeling efficiencies by 14, 35, and 41%, respectively, suggesting that KTP can also bind to GSK3α, albeit at a weaker affinity than ATP (Figure 4d–f). Similar results were obtained for GSK3β, although the extents of decreases differ somewhat from what we found for GSK3α (Figure S5). These results

suggest that the alterations in ATP probe labeling efficiency can allow for determination of relative binding affinities of ATP analogues toward kinases. The quantitative results for other kinases are listed in Tables S1 and S2.

N^6-Me-ATP, but Not KTP, Could Support the GSK3β- Mediated Phosphorylation Reaction *In Vitro*.

Kinases catalyze the transfer of the γ phosphate in ATP to their substrate proteins or small molecules. The aforementioned chemoproteomic results revealed that the two ATP analogues exhibit appreciable binding affinities toward GSK3α and GSK3β. Hence, we next conducted an *in vitro* kinase assay to examine whether the two ATP analogues can serve as phosphate group donors for GSK3β.

While GSK3 can phosphorylate directly a few nonprimed substrates with the target serine preceding a proline residue, most common targets for GSK3-mediated phosphorylation reside in a sequence of S/T-X-X-X-S/T(P), where the kinase phosphorylates a serine or threonine four residues N-terminal to a prephosphorylated serine/threonine.[34] Hence, we performed the *in vitro* phosphorylation reaction by incubating recombinant GST-GSK3β (see the Experimental Section and Figures S2, S3) with a primed substrate peptide, YRRAAVPPSPSLSRHSSPHQ(pS)EDEEE, which was derived from glycogen synthase 1, together with the same concentrations of ATP, N^6-Me-ATP, or KTP. We subsequently monitored the reaction mixtures using LC-MS/MS and compared the relative levels of phosphorylation based on the relative abundances of the $[M + 3H]^{3+}$ ions of the mono-, di-, and tri-phosphorylated forms of the GSK3β substrate peptide (Figure 5a–c and S6). Our results showed that KTP is not a desirable phosphate group donor, with only 6.6% substrate peptide being phosphorylated. Under the same experimental conditions, N^6-Me-ATP, however, enabled the phosphorylation of 67.8% of the substrate peptide, which is very similar as ATP in enabling the GST-GSK3β-mediated phosphorylation of its substrate peptide (Figure 5d).

MD Simulation for Understanding the Differences of N^6-Me-ATP and KTP in Mediating the GSK3β-Mediated Phosphorylation.

Our above proteomic data revealed that both N^6-Me-ATP and KTP are capable of competing with ATP in binding toward GSK3; only the former ATP analogue, however, could strongly support the GSK3-mediated *in vitro* kinase reaction. To understand the molecular origins of these differences, we first examined if the three ligands can stably occupy the ATP-binding pocket of the kinase. Generally, proteins with an unfit ligand inside the binding pocket rearrange much more extensively than that bound tightly with a ligand. Our flexible docking experiments showed that the binding free energy for the GSK3β-N^6-Me-ATP complex is −17.30 kcal/mol, which is similar to that of the GSK3β-ATP complex (−18.74 kcal/mol) but lower than that of the KTP–GSK3β complex (−13.04 kcal/mol). From the docking results, the phosphate group of N^6-Me-ATP recapitulates what was observed for that of ATP in its complex with GSK3β; however, the phosphate group of KTP would curl into the binding pocket, which prevented itself from substrate engagement (Figure S7). Hence, the docking results are consistent with our experimental observations, that is, N^6-Me-ATP can support GSK3β-mediated phosphorylation of its substrate peptide.

While molecular docking is a powerful method for examining protein-ligand interactions, protein dynamics provides molecular insights into kinase functions. Therefore, we conducted MD simulations to examine the activation loop dynamics and interactions between the kinase and the three ATP derivatives. We first quantified protein conformational flexibility by calculating protein backbone root-mean-square-fluctuation (RMSF) with a restrained ligand position during MD simulations. In this vein, increased protein motion leads to large RMSF values. As illustrated in Figure S8, GSK3β formed stable complexes with ATP and N^6-Me-ATP; upon binding with the two ligands, the kinase exhibited very similar fluctuation. GSK3β, however, fluctuates more substantially upon binding with KTP, especially in the loop regions near amino acid residues Ile240 and Ala300. Because these two loop regions do not participate in interactions that are essential for stable ligand binding at the active site, the loop motion unlikely affects the binding of KTP with GSK3β.[35] Thus, the MD simulation results suggest that ATP, KTP, and N^6-Me-ATP can all fit nicely into the ATP-binding pocket of GSK3β.

We next investigated the activation loop position to explore whether GSK3β can adopt an active conformation upon binding with the three nucleotides. When a kinase is catalytically competent, its activation loop needs to be in an active conformation for phosphate transfer. The active conformation is similar among different kinases; therefore, we used an active loop conformation of CDK2 (PDB ID: 1QMZ) as a reference structure for catalytically active forms of kinases. We subsequently compared the loop of GSK3β complexes with the reference structure to examine the enzymatic activity (Figure 6a). During the entire course of MD run, the loop of the N^6-Me-ATP-GSK3β complex remained in an active position, similar to that of CDK2 (Figure 6b), suggesting that GSK3β can efficiently employ N^6-Me-ATP to phosphorylate its substrate.

Unlike the N^6-Me-ATP-GSK3β complex, active loop conformations of ATP-GSK3β and KTP-GSK3β existed, but the loop did not stay in the active configuration all the time. For example, in the first 32 ns of the MD run, the loop of the ATP-GSK3β complex was in an active configuration. Tyr216 of the loop subsequently formed hydrogen bonds (H-bonds) with ATP to hinder substrate binding for catalysis (Figure 6c). In this vein, it is worth noting that phosphorylated Tyr216, which increases the catalytic activity of GSK3β by approximately 200-fold,[36] is unlikely capable of forming H-bonds with ATP. Moreover, the H-bond between Tyr216 and ATP is exposed to the solvent and can be disrupted by water molecules, which allows the loop to restore to an active position. Therefore, the ATP-GSK3β complex is catalytically active. The loop of KTP-GSK3β was also in the active form during the initial period of the MD run. After a 15 ns MD simulation, Cys218 of the loop started to form H-bonds with KTP, which prohibits the loop from being accessed by a natural substrate (Figure 6d). The H-bond between Cys218 and KTP is more stable than that formed between Tyr216 and ATP. As a result, the dynamics of the activation loop suggests that, although the GSK3β-KTP complex can still be catalytically competent, its catalytic activity should be substantially reduced, which is in line with our results obtained from the *in vitro* biochemical assay. A close-up view of interactions between ATP, KTP, and N^6-Me-ATP with GSK3β at different time steps (0, 15, 32, and 50 ns) can be found in Figures S9–Sll.

CONCLUSIONS

We employed a chemoproteomic approach based on the use of stable isotope-labeled ATP-affinity probes and scheduled MRM, to identify, at the proteome-wide level, kinase proteins that can bind to two N^6-modified ATP derivatives, that is, N^6-Me-ATP and KTP. To the best of our knowledge, this is the first kinome-wide assessment about the interactomes of N^6-Me-ATP and KTP.

Kinases have long been shown to serve as central regulators of many crucial cellular processes including metabolism, membrane transport, gene expression, DNA repair, and cellular differentiation.[4,5] KTP was also identified as a neosubstrate for increasing the activity of PINK1, which may constitute a novel approach for modulating kinase activity and drug discovery. Here, our chemoproteomic approach led to the identifications of 27 and 18 putative kinases that can be targeted by KTP and N^6-Me-ATP, respectively. Many of these kinases are disease-related, for example, GSK3α, GSK3β, and eEF2K, as noted above. Therefore, our results revealed that the two ATP analogues can be recognized by a good number of endogenous kinases. This observation, hence, also calls for comprehensive characterizations of the interactions between the entire kinome and ATP/purine analogues when these analogues are employed in combination with engineered kinases for identifying direct substrates of kinases.

We also compared the relative binding affinities of kinases toward the ATP analogues and ATP. By employing different N^6-Me-ATP or KTP over ATP probe ratios of 1:10, 1:1, and 2:1, we observed progressive diminutions in ATP probe labeling efficiencies for many identified kinases. In this vein, the extent of labeling for GSK3α indicates that it has a very similar binding affinity to N^6-Me-ATP and ATP. With the *in vitro* kinase assay, we further validated the ability of N^6-Me-ATP to serve as the phosphate group donor for GSK3β-catalyzed phosphorylation of its substrate peptide.

By employing MD simulations, we found that N^6-Me-ATP–GSK3β, ATP-GSK3β, and KTP-GSK3β complexes might all exist, but the activation loop position of KTP-GSK3β suggests the KTP-occupied GSK3β does not always assume an active conformation to support its enzymatic activity.

Together, our chemoproteomic strategy allows for identification of the specific endogenous kinases that could accept unnatural N^6-modified ATP analogues, which provides important knowledge for developing small-molecule inhibitors or activators of kinases, and for manipulating kinase-dependent bio-orthogonal systems via specific ATP analogue(s). It can be envisaged that this method can be adapted for uncovering kinases that can be targeted by other purine analogues and their nucleotide metabolites, for example, 2-aminopurine and plant cytokinins.[37,38] We also expect that exploring further the biological effects modulated by ATP analogues may afford new venues for treating diseases resulting from dysregulated kinases.

Supplementary Material

Refer to Web version on PubMed Central for supplementary material.

ACKNOWLEDGMENTS

This work was supported by the National Institutes of Health (R01 CA210072 to Y.W. and R01 GM109045 to C.C.).

REFERENCES

(1). Rauch J; Volinsky N; Romano D; Kolch W Cell Commun. Signal. 2011, 9, 23–28. [PubMed: 22035226]

(2). Roskoski R Pharmacol. Res. 2015, 100, 1–23. [PubMed: 26207888]

(3). Wilson LJ; Linley A; Hammond DE; Hood FE; Coulson JM; MacEwan DJ; Ross SJ; Slupsky JR; Smith PD; Eyers PA; Prior IA Cancer Res. 2018, 78, 15–29. [PubMed: 29254998]

(4). Blume-Jensen P; Hunter T Nature 2001, 411, 355–365. [PubMed: 11357143]

(5). Lemmon MA; Schlessinger J Cell 2010, 141, 1117–1134. [PubMed: 20602996]

(6). Ardito F; Giuliani M; Perrone D; Troiano G; Muzio LL Int. J. Mol. Med. 2017, 40, 271–280. [PubMed: 28656226]

(7). Newman RH; Hu J; Rho H-S; Xie Z; Woodard C; Neiswinger J; Cooper C; Shirley M; Clark HM; Hu S; Hwang W; Seop Jeong J; Wu G; Lin J; Gao X; Ni Q; Goel R; Xia S; Ji H; Dalby KN; Birnbaum MJ; Cole PA; Knapp S; Ryazanov AG; Zack DJ; Blackshaw S; Pawson T; Gingras AC; Desiderio S; Pandey A; Turk BE; Zhang J; Zhu H; Qian J Mol. Syst. Biol. 2013, 9, 655. [PubMed: 23549483]

(8). Bodenmiller B; Aebersold R Methods Mol. Biol. 2011, 694, 307–322. [PubMed: 21082442]

(9). Damle NP; Mohanty D Bioinformatics 2014, 30, 1730–1738. [PubMed: 24574117]

(10). Allen JJ; Li M; Brinkworth CS; Paulson JL; Wang D; Hubner A; Chou W-H; Davis RJ; Burlingame AL; Messing RO; Katayama CD; Hedrick SM; Shokat KM Nat. Methods 2007, 4, 511–516. [PubMed: 17486086]

(11). Hertz NT; Berthet A; Sos ML; Thorn KS; Burlingame AL; Nakamura K; Shokat KM Cell 2013, 154, 737–747. [PubMed: 23953109]

(12). Picotti P; Aebersold R Nat. Methods 2012, 9, 555–566. [PubMed: 22669653]

(13). Peterson AC; Russell JD; Bailey DJ; Westphall MS; Coon JJ Mol. Cell. Proteomics 2012, 11, 1475–1488. [PubMed: 22865924]

(14). Miao W; Xiao Y; Guo L; Jiang X; Huang M; Wang Y Anal. Chem. 2016, 88, 9773–9779. [PubMed: 27626823]

(15). Xiao Y; Guo L; Wang Y Anal. Chem. 2013, 85, 7478–7486. [PubMed: 23841533]

(16). Wiśniewski JR; Zougman A; Nagaraj N; Mann M Nat. Methods 2009, 6, 359–362. [PubMed: 19377485]

(17). Bertrand JA; Thieffine S; Vulpetti A; Cristiani C; Valsasina B; Knapp S; Kalisz HM; Flocco MJ Mol. Biol. 2003, 333, 393–407.

(18). Case DA; Cheatham TE; Darden T; Gohlke H; Luo R; Merz KM; Onufriev A; Simmerling C; Wang B; Woods RJ J. Comput. Chem. 2005, 26, 1668–1688. [PubMed: 16200636]

(19). Maier JA; Martinez C; Kasavajhala K; Wickstrom L; Hauser KE; Simmerling CJ Chem. Theory Comput. 2015, 11, 3696–3713.

(20). Li P; Song LF; Merz KM J. Phys. Chem. B 2015, 119, 883–895. [PubMed: 25145273]

(21). Meagher KL; Redman LT; Carlson HA J. Comput. Chem. 2003, 24, 1016–1025. [PubMed: 12759902]

(22). Jakalian A; Jack DB; Bayly CI J. Comput. Chem. 2002, 23, 1623–1641. [PubMed: 12395429]

(23). Hawkins GD; Cramer CJ; Truhlar DG J. Phys. Chem. 1996, 100, 19824–19839.

(24). Hawkins GD; Cramer CJ; Truhlar DG Chem. Phys. Lett. 1995, 246, 122–129.

(25). Ryckaert J-P; Ciccotti G; Berendsen HJC J. Comput. Phys. 1977, 23, 327–341.

(26). Escher C; Reiter L; MacLean B; Ossola R; Herzog F; Chilton J; MacCoss MJ; Rinner O Proteomics 2012, 12, 1111–1121. [PubMed: 22577012]

(27). Hanger DP; Hughes K; Woodgett JR; Brion J-P; Anderton BH Neurosci. Lett. 1992, 147, 58–62. [PubMed: 1336152]

(28). Mandelkow E-M; Drewes G; Biernat J; Gustke N; Van Lint J; Vandenheede JR; Mandelkow E FEBS Lett. 1992, 314, 315–321. [PubMed: 1334849]

(29). Stambolic V; Ruel L; Woodgett JR Curr. Biol. 1996, 6, 1664–1669. [PubMed: 8994831]

(30). Klein PS; Melton DA Proc. Natl. Acad. Sci. U.S.A. 1996, 93, 8455–8459. [PubMed: 8710892]

(31). Machado-Vieira R; Manji HK; Zarate CA Jr. Bipolar Disord. 2009, 11,92–109. [PubMed: 19538689]

(32). Wang X; Xie J; Proud C Cancers 2017, 9, 162.

(33). Bowie LE; Maiuri T; Alpaugh M; Gabriel M; Arbez N; Galleguillos D; Hung CLK; Patel S; Xia J; Hertz NT; Ross CA; Litchfield DW; Sipione S; Truant R Proc. Natl. Acad. Sci. U.S.A. 2018, 115, E7081–E7090. [PubMed: 29987005]

(34). Beurel E; Grieco SF; Jope RS Pharmacol. Ther. 2015, 148, 114–131. [PubMed: 25435019]

(35). Brown NR; Noble MEM; Endicott JA; Johnson LN Nat. Cell Biol. 1999, 1, 438–443. [PubMed: 10559988]

(36). Hughes K; Nikolakaki E; Plyte SE; Totty NF; Woodgett JR EMBO J. 1993, 12, 803–808. [PubMed: 8382613]

(37). Hu Y; Conway TW J. Interferon Res. 1993, 13, 323–328. [PubMed: 7905506]

(38). Mok DW; Mok MC Annu. Rev. Plant Physiol. Plant Mol. Biol. 2001, 52, 89–118. [PubMed: 11337393]

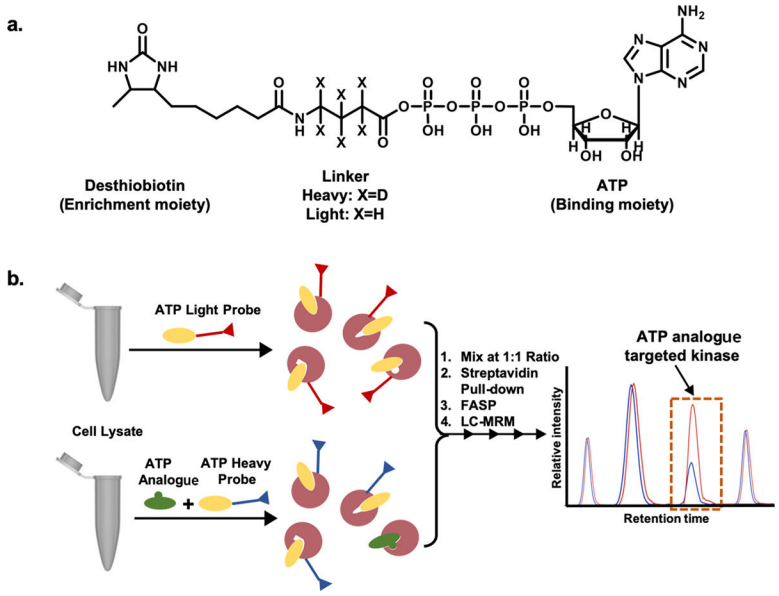

Figure 1.

hemoproteomic strategy for proteome-wide assessment of the binding capabilities of kinases toward ATP analogues. (a) Chemical structures of isotope-labeled ATP affinity probes; (b) competition strategy for quantitative discovery of ATP analogue-targeted kinases using stable isotope-coded ATP probes.

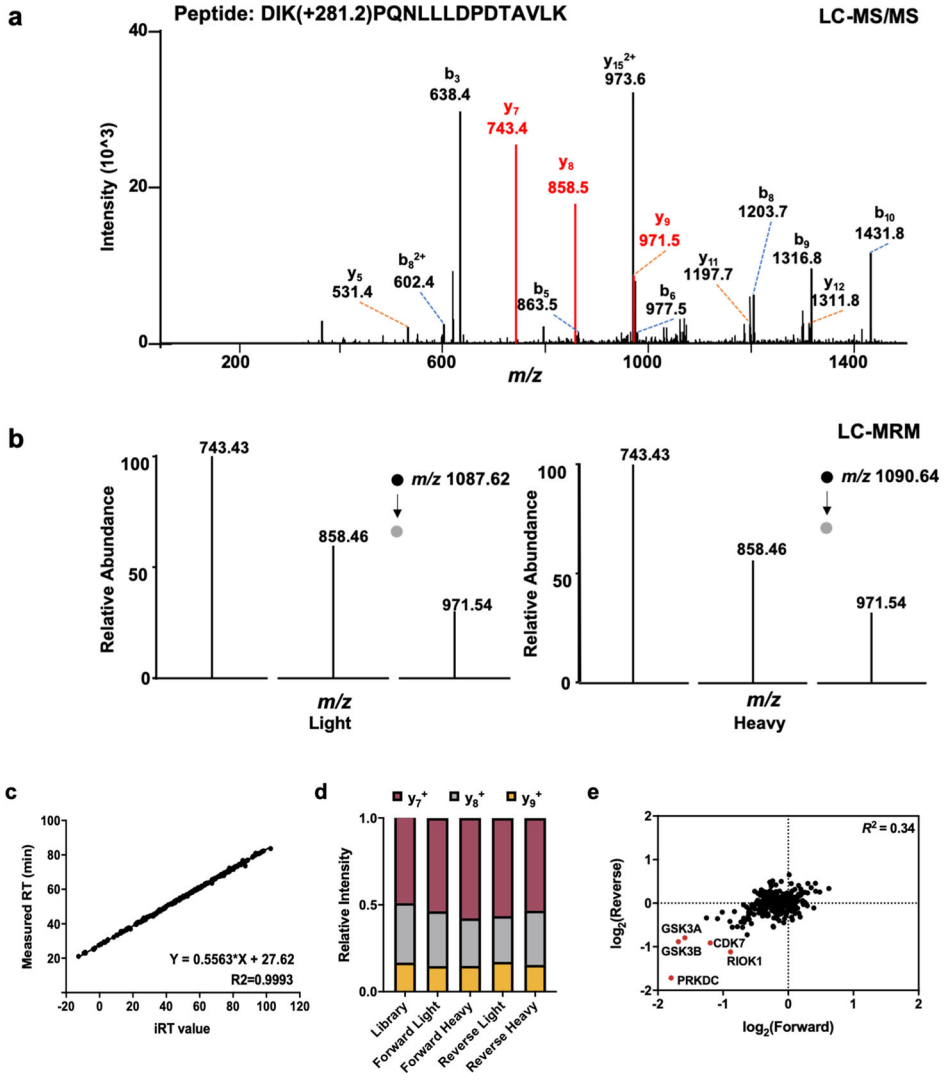

Figure 2.

Performance of the LC-MRM-based method for quantitative profiling of the binding capabilities of kinases toward N^6-Me-ATP and KTP. (a) Representative MS/MS of a probe-labeled tryptic peptide from GSK3β, y ions labeled in red represent the three transitions used for MRM analysis; (b) MS/MS of light and heavy precursors with the selected three transitions acquired from the LC-MRM experiment; (c) Scatter plot showing the correlation between the observed retention times for desthiobiotin-labeled kinase peptides and their normalized retention times (iRTs) in the kinome MRM library; (d) Relative abundances of three fragment ions observed in DDA (labeled as 'Library') and MRM analyses (from forward and reverse probe labeling experiments); (e) Comparison of quantification results obtained from forward and reverse N^6-Me-ATP competition labeling experiments.

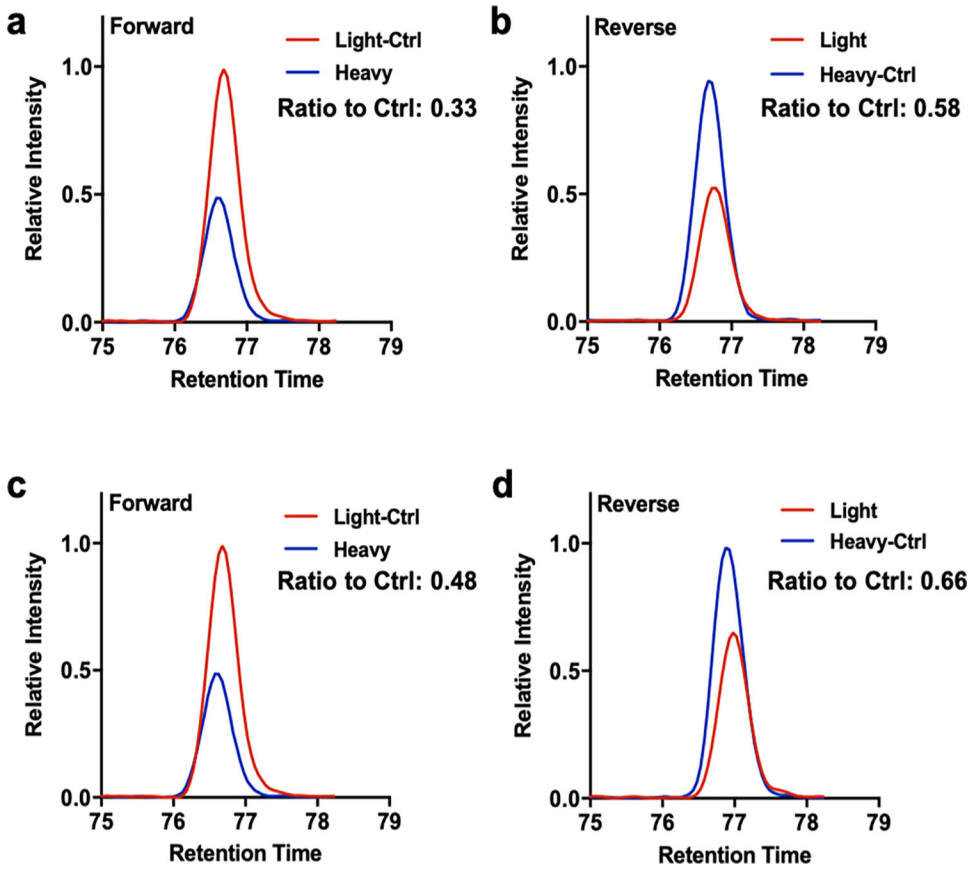

Figure 3.

MRM traces for the light and heavy forms of the probe-labeled peptide from GSK3α obtained from forward and reverse probe labeling experiments. (a-d) Selected-ion chromatograms for a tryptic peptide of GSK3α obtained from N^6-Me-ATP (a,b) and KTP (c,d) competition experiments. In forward and reverse labeling experiments, protein lysates preincubated with 100 μM N^6-Me-ATP or KTP were labeled with the heavy and light desthiobiotin-ATP acyl-phosphate probes, respectively, whereas the protein lysates without preincubation with the ATP analogues were labeled with the light and heavy stable isotope-labeled forms of desthiobiotin-ATP acyl-phosphate probe, respectively. The quantification results, as reflected by labeling ratios, obtained from LC-MRM analyses are listed in each panel.

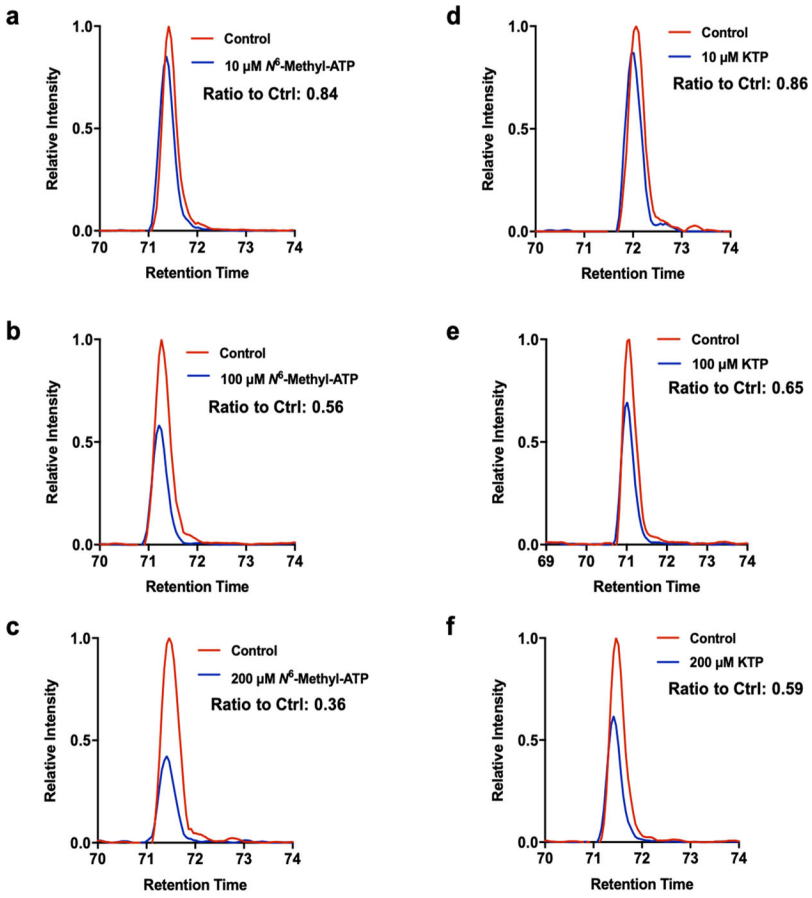

Figure 4.

MRM traces for probe-labeled peptide from GSK3α obtained from N^6-modified ATP analogue concentration-dependent competition experiments. (a-f) Selected-ion chromatograms obtained from the competition experiments, where the heavy lysate was preincubated with 10, 100, and 200 μM N^6-Me-ATP (a-c) or KTP (d-f) prior to labeling with the heavy ATP acyl-phosphate probe, whereas the light lysate without the ATP analogue was labeled with the light ATP acyl-phosphate probe. The quantification results, as reflected by labeling ratios, obtained from LC–MRM analyses are listed in each panel.

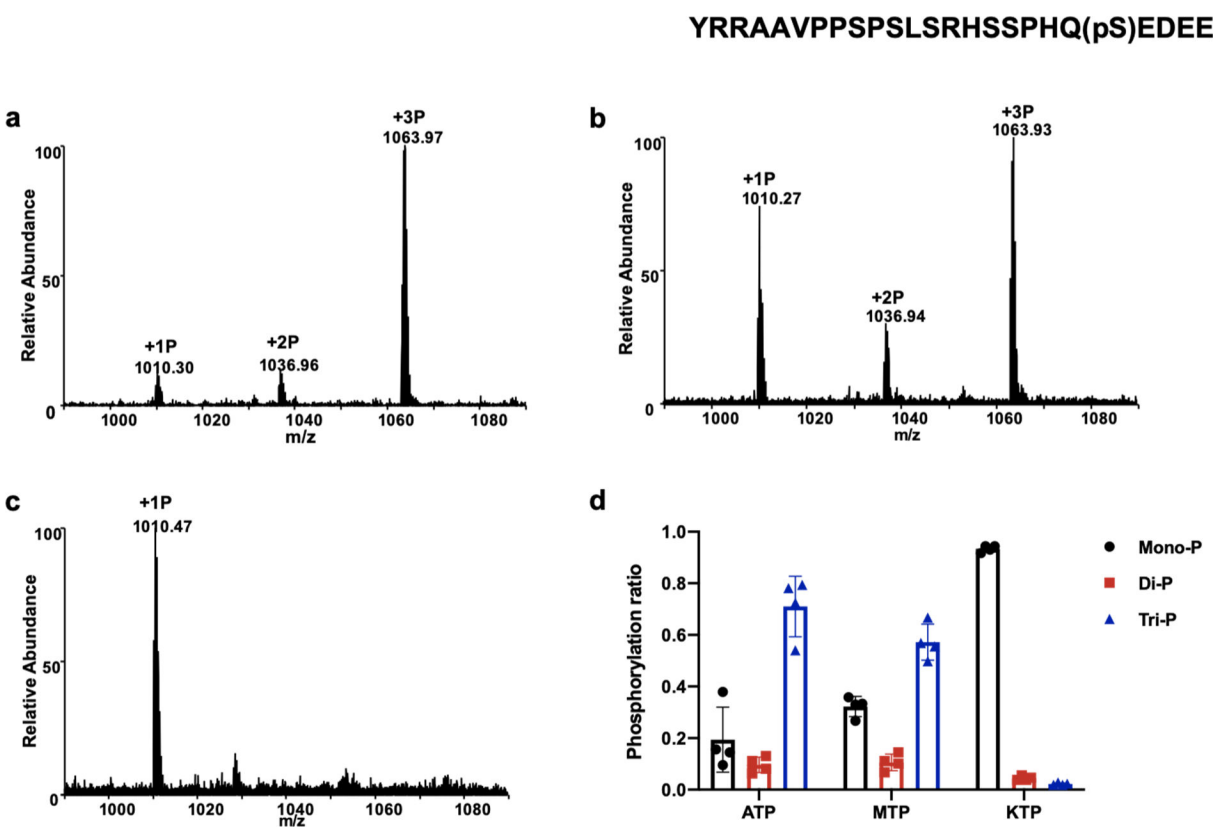

Figure 5.

In vitro kinase assay of GSK3β with a phosphopeptide substrate of the kinase. GST-GSK3β (1.0 μM) was incubated with 10 μM of its peptide substrate derived from glycogen synthase along with 250 μM ATP, N^6-Me-ATP, or KTP at 37 °C for 2 h. GSK3β kinase activity was assayed using the conversion ratio of the relative abundances of the mono-, di-, and tri-phosphorylated forms of the glycogen synthase peptide. (a–c) "Ultrazoom" scan ESI-MS for the $[M + 3H]^{3+}$ ions of the different phosphorylated forms of the glycogen synthase peptide from the *in vitro* kinase reactions with the use of ATP (a), N^6-Me-ATP (b), or KTP (c) as phosphate group donors. (d) Comparison of relative GSK3β activities with the use of different ATP derivatives, as represented by different phosphorylated forms of its substrate peptide.

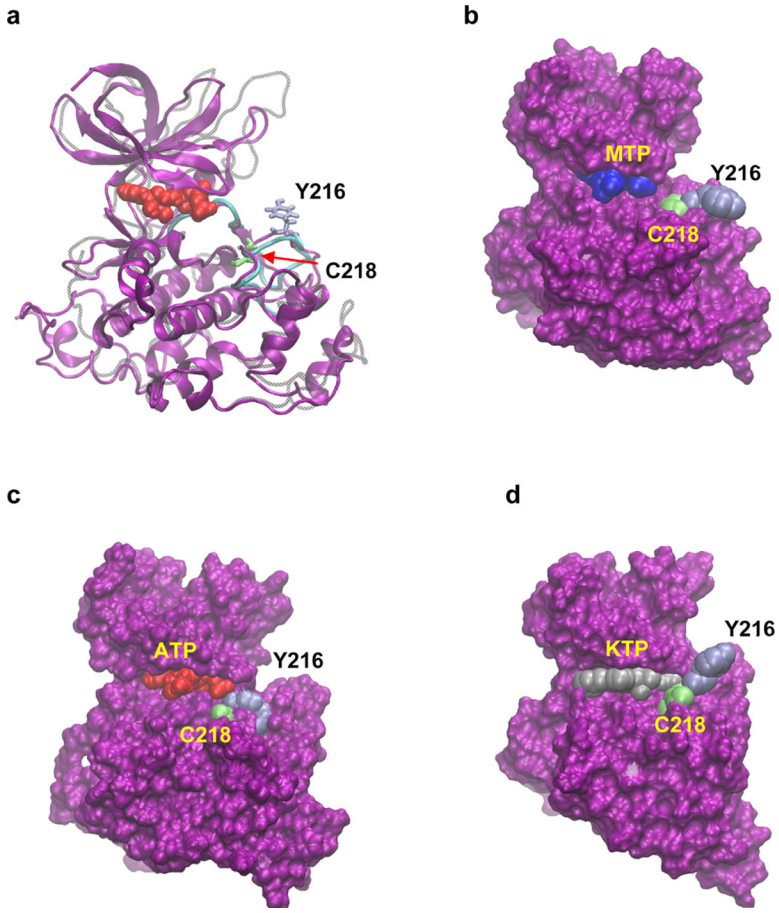

Figure 6.

Conformations of GSK3β-ligand complexes. (a) Superimposed GSK3β (purple) with CDK2 (gray). ATP (red) is in van der Waals representation. Two residues in the GSK3β activation loop, Tyr216 (ice blue), and Cys218 (light green), are shown in licorice representation. Activation loop in CDK2 is in cyan. (b) GSK3β (purple) with N^6-Me-ATP (blue), Tyr216 (ice blue), and Cys218 (light green). (c) GSK3β with ATP (red), Tyr216, and Cys218. (d) GSK3β with KTP (silver), Tyr216, and Cys218.

Table 1.

Candidate Kinase Proteins with Capabilities in Binding toward KTP

protein accession	protein gene	mean ratio	S.D.
Q16513	PKN2	0.54	0.22
O00418	EEF2K	0.60	0.19
P30876	POLR2B	0.61	0.30
P49840	GSK3A	0.61	0.16
Q9NWZ3	IRAK4	0.65	0.16
Q9Y2K2	SIK3	0.66	0.15
P48729	CSNK1A1	0.66	0.03
P41743	PRKCI	0.68	0.15
Q9H8X2	IPPK	0.69	0.05
Q9UJ70	NAGK	0.69	0.24
P78527	PRKDC	0.72	0.37
P19784	CSNK2A2	0.70	0.31
Q04759	PRKCQ	0.71	0.18
P49841	GSK3B	0.72	0.19
P54619	PRKAG1	0.72	0.22
P48426	PIP4K2A	0.72	0.34
Q96GX5	MASTL	0.72	0.51
Q8IWY7	TTBK2	0.73	0.02
Q5VST9	OBSCN	0.73	0.26
Q13263	TRIM28	0.73	0.31
P46734	MAP2K3	0.74	0.23
Q9P0L2	MARK1	0.74	0.20
Q9BYT3	STK33	0.74	0.01
P00558	PGK1	0.74	0.78
Q14680	MELK	0.74	0.15
P50750	CDK9	0.74	0.01
Q99538	LGMN	0.75	0.30

Table 2.

Candidate Kinase Proteins with Capabilities in Binding toward *N*6-Me-ATP

protein accession	protein gene	mean ratio	S.D.
Q9BRS2	RIOK1	0.50	0.06
P78527	PRKDC	0.51	0.24
P49841	GSK3B	0.54	0.17
P49840	GSK3A	0.55	0.16
P50613	CDK7	0.59	0.13
Q16513	PKN2	0.60	0.26
Q9P0L2	MARK1	0.63	0.03
Q14680	MELK	0.65	0.17
Q9H477	RBKS	0.68	0.08
O00418	EEF2K	0.69	0.19
Q96S44	TP53RK	0.70	0.13
P48729	CSNK1A1	0.70	0.12
Q9Y2K2	SIK3	0.71	0.09
Q15349	RPS6KA2	0.72	0.22
P53350	PLK1	0.72	0.48
O75676	RPS6KA4	0.73	0.50
P43405	SYK	0.74	0.19
Q9BZL6	PRKD2	0.74	0.12